Simultaneous convection and radiation in flow between two parallel plates

M. M. Elsayed and K. A. Fathalah*

A numerical solution is described for simultaneous forced convection and radiation in flow between two parallel plates forming a channel. The front plate is transparent to thermal radiation while the back one is thermally insulated. Analyses for both flow and heat are presented for the case of a non-emitting 'blackened' fluid. The governing equations of the stream function and the temperature together with their boundary conditions are presented in non-dimensional expressions. The solution is found to depend on eight dimensionless parameters, namely the ratio of the height of the channel to the distance between the plates, the initial dimensionless temperature, the optical thickness, the absorptivities of both plates, the Reynolds number, the Prandtl number and the heat transfer coefficient from the front plate to the surroundings. The numerical solution is obtained using a finite-difference technique. A study has been made of the effect of the initial temperature of the flow at the channel inlet, the dimensionless loss coefficient from the front plate, the absorptivity of the back plate and the optical thickness, on the temperature distribution in the channel, the heat collection efficiency and the average temperature rise in the channel. Results showed that increasing the optical thickness increases the temperature of the front plate and decreases the temperature of the back plate. Also, increasing the optical thickness increases the efficiency of heat collection, which reaches its maximum asymptotic value at an optical thickness of about 1.5. Moreover, the location of the maximum temperature is found to depend on both the optical thickness and the dimensionless heat loss coefficient from the front plate.

Key words: *convection, radiation, channel flow, solar collectors*

Flow in ducts with combined convection and radiation is of great importance in many industrial and engineering applications, including high-temperature heat exchangers, furnaces, nuclear reactors, solar collectors and many others. Many established models in the literature explore the distributions of both velocity and temperature as well as the heat transfer coefficient between the walls of the ducts and the flow. Although different shapes of duct are commonly used in engineering problems, most of the attention of researchers has been given to flow inside a pipe or between two plates. Both laminar and turbulent flows have been considered, with various assumptions regarding the velocity field, the temperature field, the optical thickness and the radiation properties of the medium.

Laminar flow in a pipe was studied by Desoto and Edwards[1], DeSoto[2], Pearce and Emery[3] and Wassel and Edwards[4], while turbulent flow inside pipes was investigated by Landram *et al*[5] and Wassel and Edwards[4]. Pearce and Emery[3] assumed non-grey gases with constant absorption coefficient over an effective bandwidth and zero absorption coefficient elsewhere. Tubes with constant wall heat flux were considered by Landram *et al*[5], Clausen and Smith[6], and Smith and Clausen[7], while those of specified wall temperature were investigated by Wassel and Edwards[4]. DeSoto and Edwards[1] assumed temperature-dependent radiation properties. Landram *et al*[5] assumed fully developed hydrodynamic and thermal distributions in addition to an optically thin gas.

There have been many investigations of flow between two parallel plates. Laminar flow was assumed by Chawla and Chen[8], Lii and Ozisik[9], Viskanta[10], Balakrishnan and Edwards[11], Liu and Thorsen[12], Chen[13], Kurosaki[14], Chawla *et al*[15] and Greif and McEligot[16]. Fully developed velocity and/or temperature fields were assumed by Chawla and Chen[8], Viskanta[10], Liu and Thorsen[12] and Greif and McEligot[16]. A scattering medium was examined by Chawla and Chen[8], Lii and Ozisik[9], Chen[13] and Chawla *et al*[15].

A common feature of all these investigations is that they deal with the problem of radiation and convection interchange between a gas and a bounding wall (or walls) of specified temperature or heat

* Mechanical Engineering Department, King Abdulaziz University, PO Box 9027, Jeddah, Saudi Arabia
Received 5 February 1982 and accepted for publication on 22 April 1982

flux. In contrast, the work described here assumes one plate to be transparent, and the other plate to be thermally insulated from the surroundings. A 'blackened' fluid that flows between the two plates will directly absorb the radiation transmitted through the transparent plate and thermally interact with both the bounding walls. The work is an extension of previous work[17,18] on simultaneous convection and radiation in flow over transparent flat plates. The main application of the present work is in the design of direct solar collectors with absorbing fluid rather than an absorbing plate.

Analysis

Consider the flow between two parallel plates forming a channel at a distance b apart from each other as shown in Fig 1. The two plates are of infinite width. The back plate is thermally insulated and has an absorptivity α_b. The front plate is thermally insulated near the top to a distance $\bar{H}_1$ from the top and the rest of the plate is transparent to radiation. The reason for including the insulated part $\bar{H}_1$ is to generalise the model to make it relevant to a wide range of applications where the height $\bar{H}_1$ may be greater than or equal to zero. The front plate has an absorptivity α_f and transmissivity τ and it is exposed to

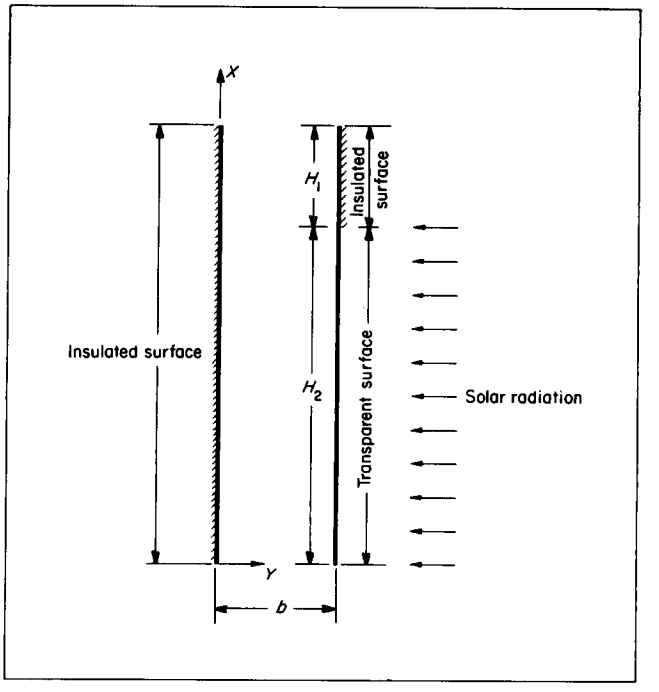

Fig 1 Channel flow with simultaneous convection and radiation

Nomenclature

a	Absorption coefficient per unit thickness of the fluid layer, m^{-1}
b	Distance between the front and back plates (see Fig 1), m
B	Dimensionless heat transfer coefficient between front plate and surroundings ($=hb/k$)
c	Specific heat of the fluid, J/kg K
g	Gravitational acceleration, m/s^2
$\dot{G}$	Mass flow rate per unit area of the transparent part of the front plate, kg/m^2 s
h	Heat transfer coefficient between front plate and surroundings, W/m^2 K
$\bar{H}_1, \bar{H}_2$	Heights of the channel (see Fig 1), m
H_1, H_2	Dimensionless heights of the channel (normalised by distance between the two plates)
k	Thermal conductivity of the fluid, W/m K
Pr	Prandtl number of the fluid ($=\mu c/k$)
q''	Incident radiation heat flux per unit area of the front plate, W/m^2
Q_r	Heat removed by the flow up to any distance from the channel inlet per unit width of the channel (see Eq 10), W/m
Re	Reynolds number of the flow ($=\dot{G}\bar{H}_2/\mu$)
T	Temperature of flow at any location, K
u	Longitudinal velocity, m/s
U	Dimensionless longitudinal velocity ($=\partial\Psi/\partial Y$)
v	Normal velocity, m/s
x	Coordinate along the channel (see Fig 1), m
X	Dimensionless coordinate along the channel
y	Coordinate normal to the channel (see Fig 1), m
Y	Dimensionless coordinate normal to the channel
Z	Dimensionless vorticity (see Eq 5)
α	Plate absorptivity
β	Coefficient of volumetric expansion per unit volume of the fluid, K^{-1}
ζ	Vorticity, s^{-1}
η	Heat collection efficiency (see Eq 11)
θ	Dimensionless temperature (see Eq 5)
μ	Dynamic viscosity of the fluid, $N\,s/m^2$
ρ	Density of the fluid, kg/m^3
τ	Transmissivity of the front plate
ψ	steam function, kg/m s
Ψ	Dimensionless steam function (see Eq 5)

Subscripts

av	average
b	back plate
e	exit of channel
f	front plate
i	inlet to channel
∞	surroundings

surroundings at an average temperature T_∞. When an absorbing fluid flows between the two plates, a part of the solar radiation transmitted from the front plate is absorbed by the fluid and the rest undergoes absorption and reflection by the back plate. The radiation reflected from the back plate is attenuated by absorption in the fluid and as it reaches the front plate it is assumed to be transmitted to the surroundings. Assuming two-dimensional flow with constant properties, the governing equations for the vorticity ζ, stream function ψ and the temperature T at steady state conditions are

$$\frac{\partial}{\partial x}\left(\zeta\frac{\partial\psi}{\partial Y}\right)-\frac{\partial}{\partial Y}\left(\zeta\frac{\partial\psi}{\partial x}\right)-\mu\left(\frac{\partial^2\zeta}{\partial x^2}+\frac{\partial^2\zeta}{\partial y^2}\right)=0 \tag{1}$$

$$\frac{\partial}{\partial x}\left(T\frac{\partial\psi}{\partial y}\right)-\frac{\partial}{\partial y}\left(T\frac{\partial\psi}{\partial x}\right)-\frac{k}{c}\left(\frac{\partial^2T}{\partial x^2}+\frac{\partial^2T}{\partial y^2}\right)$$
$$-\frac{q''}{c}a\tau\,e^{-a(b-y)}-\frac{q''}{c}a\tau(1-\alpha_b)\,e^{-a(b+y)}=0 \tag{2}$$

$$-\frac{1}{\rho}\frac{\partial^2\psi}{\partial x^2}-\frac{1}{\rho}\frac{\partial^2\psi}{\partial y^2}-\zeta=0 \tag{3}$$

where the stream function ψ is defined in terms of the velocity along the plates and normal to the plates, u and v respectively, as follows:

$$\rho u=\frac{\partial\psi}{\partial y}$$

$$\rho v=-\frac{\partial\psi}{\partial x} \tag{4}$$

The last term of Eq (2) represents the radiation absorption term. The term is derived[17,18] by using Beer's law for a cold grey (non-emitting) fluid layer of thickness b.

Table 1 Boundary conditions for Eqs (6)–(8)

Location	Variable		
	Z	Ψ	θ
Flow inlet	$Z=0$	$\frac{\partial\Psi}{\partial X}=0$	$\theta=\frac{(T_i-T_\infty)k}{q''b}=\theta_i$
Front plate, transparent part	$Z=-\frac{\partial^2\psi}{\partial Y^2}$	$\Psi=$ const	$\frac{\partial\theta}{\partial Y}=\alpha_f-B\theta_f$
Front plate, insulated part	$Z=-\frac{\partial^2\psi}{\partial Y^2}$	$\Psi=$ const	$\frac{\partial\theta}{\partial Y}=0$
Flow exit	$\frac{\partial Z}{\partial X}=0$	$\frac{\partial\Psi}{\partial X}=0$	$\frac{\partial\theta}{\partial X}=0$
Back plate $(H_2<Y<H_1+H_2)$	$Z=-\frac{\partial^2\psi}{\partial Y^2}$	$\Psi=0$	$\frac{\partial\theta}{\partial Y}=0$
Back plate $(Y\leq H_2)$	$Z=-\frac{\partial^2\psi}{\partial Y^2}$	$\Psi=0$	$\frac{\partial\theta}{\partial Y}=-\tau\alpha_b\,e^{-ab}$

The governing equations (Eqs (1)–(3)) are now transformed to dimensionless forms, using:

$$X=\frac{x}{b}$$

$$Y=\frac{y}{b}$$

$$Z=\frac{\rho b}{G}\zeta \tag{5}$$

$$\Psi=\frac{\Psi}{Gb}$$

$$\theta=\frac{(T-T_\infty)k}{q''b}$$

The transformed dimensionless equations are

$$\frac{\partial}{\partial x}\left(Z\frac{\partial\psi}{\partial Y}\right)-\frac{\partial}{\partial Y}\left(Z\frac{\partial\psi}{\partial x}\right)-\frac{H_2}{R_e}\left(\frac{\partial^2Z}{\partial x^2}+\frac{\partial^2Z}{\partial Y^2}\right)=0$$
$$\frac{\partial}{\partial x}\left(\theta\frac{\partial\psi}{\partial Y}\right)-\frac{\partial}{\partial Y}\left(\theta\frac{\partial\psi}{\partial X}\right)-\frac{H_2}{\mathrm{Pr}\times\mathrm{Re}}\left(\frac{\partial^2\theta}{\partial x^2}+\frac{\partial^2\theta}{\partial Y^2}\right) \tag{6}$$

$$-\tau(ab)\frac{1}{\mathrm{Pr}\times\mathrm{Re}}[e^{-ab(1-Y)}+(1-\alpha_b)\,e^{-ab(1+Y)}]=0 \tag{7}$$

$$-\frac{\partial^2\psi}{\partial x^2}-\frac{\partial^2\psi}{\partial Y^2}-Z=0 \tag{8}$$

The boundary conditions for Eqs (6)–(8) are given in Table 1, where

$$B=hb/k \tag{9}$$

The governing equations, Eqs (6)–(8), together with their boundary conditions may be solved by a finite-difference technique. A computer program similar to that reported by Gosman *et al*[19] was used but with slight modifications to suit the present problem. A non-uniform grid with 20 points in the x direction and 15 points in the y direction was found to be adequate for convergence with accuracy to within 0.0005 for the maximum residuals (between iterations) at any grid point.

Results

At any cross-section of distance x from the channel entrance, the heat removed per unit width of the channel is given by:

$$Q_r=\int_0^b \rho cu(T-T_i)\,dy \tag{10}$$

In terms of the dimensionless parameters defined by Eqs (5) and (9) the above equation becomes:

$$\eta=\frac{Q_r}{xq''}=\frac{Pr\times Re}{XH_2}\int_0^1 U(\theta-\theta_i)\,dY \tag{11}$$

where θ_i is the dimensionless temperature at the channel inlet, U is the dimensionless longitudinal

velocity ($=\partial\Psi/\partial Y$) and η is the efficiency of heat collection.

The average temperature of the heat-removing fluid at any cross-section is defined as:

$$T_{av} = T_i + \frac{Q_r}{\bar{H}_2 \dot{G} c} \tag{12}$$

Using Eqs (5) and (11), the above equation gives:

$$\theta_{av} = \frac{(T_{av} - T_\infty)k}{q''b} = \frac{\eta}{Re \times Pr} X + \theta_i \tag{13}$$

where H_2 is the dimensionless height of the transparent part ($=\bar{H}_2/b$). It is clear from Eqs (11) and (13) and from the analysis of the problem that the temperature distribution and the heat collection efficiency depend on eight parameters, namely H_2, θ_i, ab, α_b, Re, B, α_f and Pr. The values assigned to these parameters are given in Table 2. As is shown in the table, four of these parameters were assigned fixed values and the rest were varied as indicated.

The fixed parameters (Re, α_f, H_2 and Pr) were specified to fit solar collectors, for which the present analysis can be adopted. A solar collector with ratio $H_2 = 200$ (ratio of the collector length to the distance between the front and back plates) is chosen. The flow Reynolds number was fixed at $Re = 100$, which in practice is the order of magnitude of Re in such an application. The value of Pr was taken as 7 (ie water is used as the working fluid) and the value of α_f was fixed at 0.1 (the value expected for the type of glass normally used for solar collectors). The variable parameters—θ, B, α_b and ab—were specified to take the following ranges. The dimensionless temperature at the channel inlet took the value of 0 or 0.75 representing flow at ambient temperature and above atmospheric temperature by an amount of $0.75q''b/k$ respectively. The dimensionless heat transfer coefficient between the front plate and surroundings, B, was assigned the values of 0.1 and 1.0, which represent surroundings with still air and high wind velocity, respectively. Values of 0.5 and 0.8 were assigned for α_b, representing respectively a moderate and a high absorptivity for the back plate. The optical length was assigned values of 0.001, 0.5 and 2 to cover optically thin to optically thick layers. Table 3 summarises the values of the variable parameters as used in the computer runs.

Table 2 Values of parameters used

Parameter	Value	Parameter	Value
Re	100	ab	0.001, 0.5, 2
α_f	0.1	α_b	0.5, 0.8
H_2	200	θ_i	0, 0.75
Pr	7	B	0.1, 1

Table 3 Values of various parameters assigned to computer runs*

Run no.	θ_i	B	α_b	ab
1	0	0.1	0.5	0.001 0.5 2.0
2	0	0.1	0.8	0.001 0.5 2.0
3	0.75	0.1	0.8	0.001 0.5 2.0
4	0	1.0	0.8	0.001 0.5 2.0
5	0.75	1.0	0.8	0.001 0.5 2.0

* Values of other parameters are kept as indicated in Table 2

Discussion

The temperature distributions for optical thicknesses 0.001 and 2 are given in Fig 2 for runs 1, 2 and 4. The changes in the temperature distribution for runs 3 and 5 (where θ_i is high) are trivial and cannot be shown graphically. This indicates that most of the incident radiation is lost to the surroundings. In each run of those plotted in Fig 2, the temperature distributions are given at two stations in the channel, namely at $X = 110.9$ (marked I) and $X = 200$ (marked II). Generally, the temperature at the back plate increases with a decrease in optical thickness, because decreasing the optical thickness allows more absorption to occur at the back plate and hence increases its temperature. Conversely, the temperature of the front plate increases with an increase in optical thickness. The location of the maximum temperature in the channel depends on both the optical thickness, ab, and the dimensionless heat transfer coefficient from the outer side of the transparent plate and surroundings, B. At small optical thickness the maximum temperature is to be found at the back plate. However, if the optical thickness is increased, the maximum temperature moves from

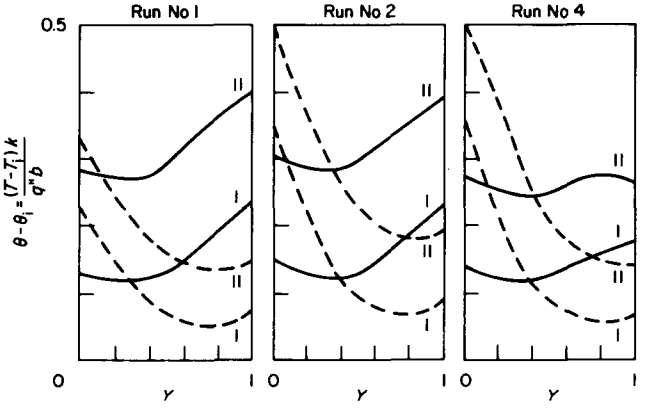

Fig 2 Temperature distribution at ab = 0.001(---) *and* ab = 2(——) *at two stations: (I) at* X = *110.9 and (II) at* X = *200 (data are plotted for runs 1, 2 and 4)*

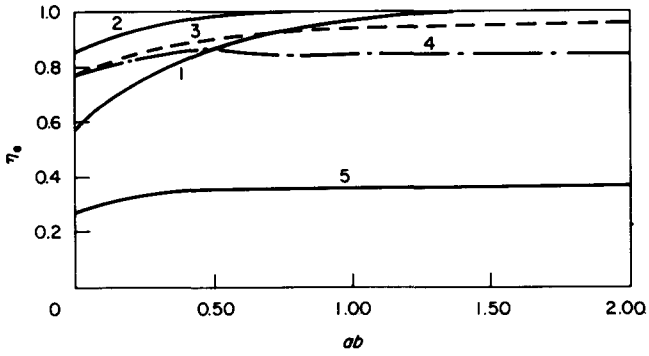

Fig. 3 Variation of the heat collection efficiency at channel exit, η_e, with optical thickness ab *(data are plotted for runs 1–5)*

the back plate, either staying in the fluid or moving to the front plate, depending on the value of B. For example, at high optical thickness, the maximum temperature is located in the fluid far from the back plate and moves closer to or even reaches the front plate as B decreases.

The variation with optical thickness of the efficiency of heat collection at the channel exit is plotted in Fig 3. The figure shows the efficiency increases with an increase in optical thickness until it reaches its asymptotic value. The dependence of the asymptotic value of η_e on the optical thickness ab varies with the parameters θ_i, B and α_b. However, although a value of 1.5 for the optical thickness is necessary to bring the efficiency to its asymptotic value under all conditions, a value of 0.5 is satisfactory for the runs having $\alpha_b = 0.8$ (a small value of α_b means that a large absorption coefficient is needed to get a high percentage of useful heat gain).

Fig 4 illustrates the change in efficiency with the distance along the channel for optical thicknesses of 0.001, 0.5 and 2. The efficiency is independent of the distance along the channel except under one of the following circumstances: (a) a high value of B and a small value of θ_i; η decreases with increase in X (run 4); or (b) high values of B and θ_i; η increases with increase in X (run 5). The worst efficiency of the channel (less than 40%) is obtained at a high value of B combined with a high value of θ_i. Reasonably good efficiency (above 80%) may be obtained under one of the following conditions: (a) low B with high α_b; (b) low θ_i with high B; or (c) large optical thickness, except for the combination high B with high θ_i.

The variation of the dimensionless temperature rise between channel inlet and exit, $(\theta_{av,e}-\theta_i)$, with optical thickness is illustrated in Fig 5 for runs 1 to 5. Very small values of $(\theta_{av,e}-\theta_i)$ are obtained when θ_i is high (runs 3 and 5). Increasing the optical thickness causes an increase in $(\theta_{av,e}-\theta_i)$ until it reaches its asymptotic value. The value of ab at which $(\theta_{av,e}-\theta_i)$ reaches its asymptotic value varies from 0.5 at a large value of α_b to 1.5 at a small value of α_b. This can be interpreted in the same way as for the efficiency. Large values of $(\theta_{av,e}-\theta_i)$ are obtained at low values of θ_i, and $(\theta_{av,e}-\theta_i)$ may be further increased by decreasing B.

The variation of $(\theta_{av}-\theta_i)$ with the distance along the channel is depicted in Fig 6. Large values

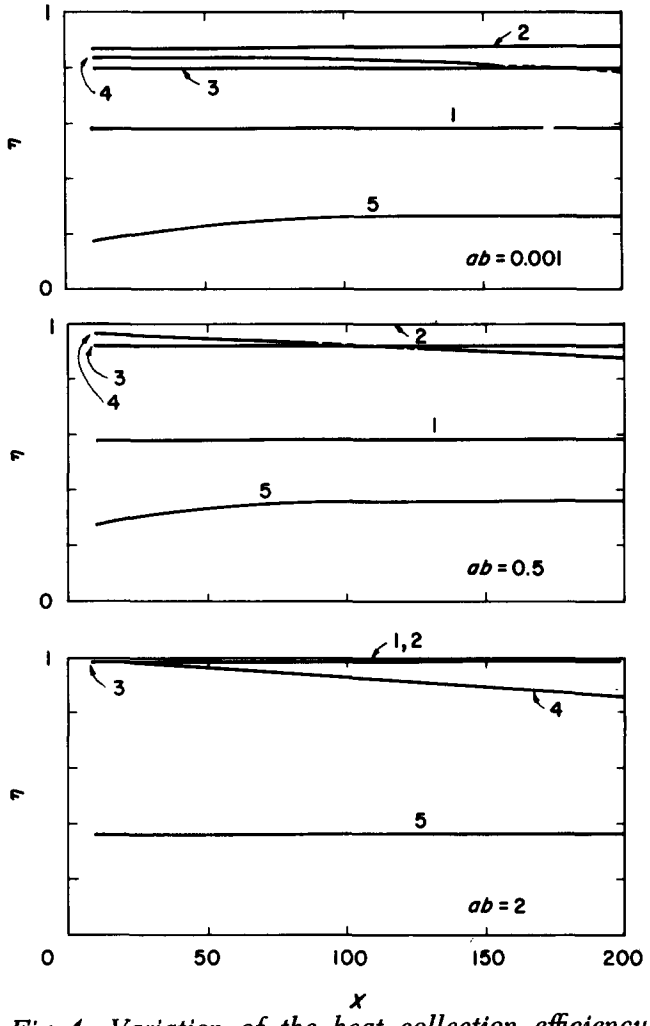

Fig 4 Variation of the heat collection efficiency with distance along the channel (data are plotted for runs 1–5)

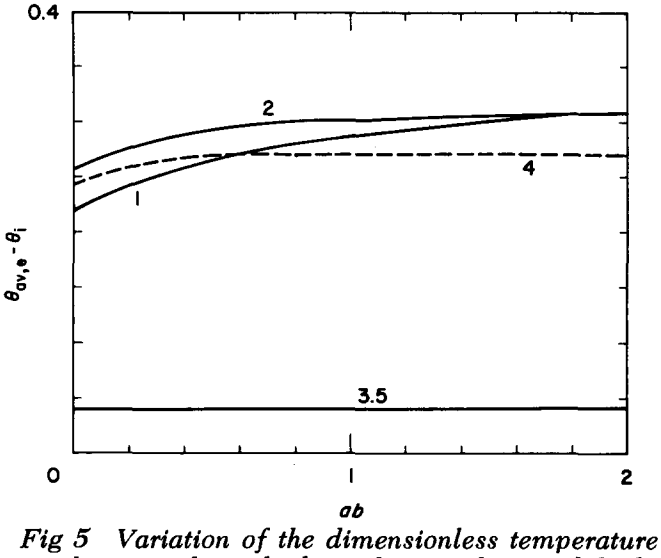

Fig 5 Variation of the dimensionless temperature rise between channel inlet and exit with optical thickness (data are plotted for runs 1–5)

of θ_i cause small variations of $(\theta_{av}-\theta_i)$ to occur through the channel. At small values of θ_i, the values of $(\theta_{av}-\theta_i)$ generally increase with X. Values of $(\theta_{av}-\theta_i)$ are further increased by either increasing α_b or decreasing B.

Conclusions

Increasing the optical thickness causes:
- an increase in the temperature of the front plate;
- a decrease in the temperature of the back plate;
- an improvement in the efficiency of heat collection, and
- an increase in the average temperature rise in the channel.

Although a value of $ab = 1.5$ appeared to be necessary for both the heat collection efficiency and the dimensionless average temperature rise in the channel to reach their asymptotic values, a value of 0.5 is satisfactory at large values of α_b.

A reasonably good efficiency (>80%) can be obtained at:
- low values of B but high values of α_b;
- high values of B but low values of θ_i, or
- large values of ab ($ab > 1.5$).

The average temperature rise in the channel is increased by:

- decreasing the value of θ_i, or
- decreasing the value of B.

The location of the maximum temperature in the flow depends on both ab and B. The location is moved closer to the front plate by increasing ab and/or decreasing B and it is moved towards the back plate by decreasing ab and/or increasing B.

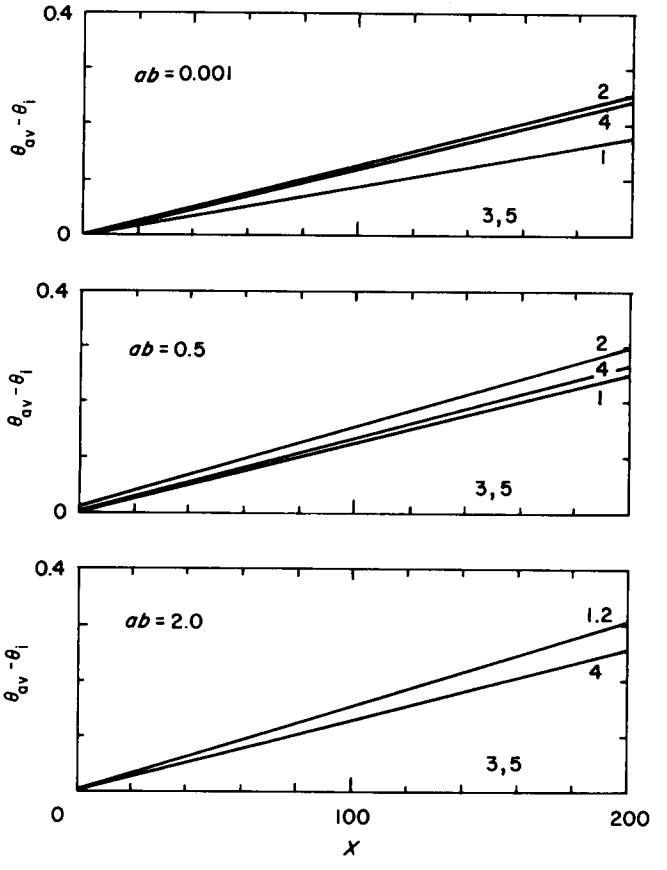

Fig 6 Variation of the dimensionless temperature rise from channel inlet with distance along the channel (data are plotted for runs 1–5)

References

1. **DeSoto S. and Edwards D K.** Radiative emission and absorption in non-isothermal nongray gases in tubes. *Proc. 1965 Heat Transfer Fluid Mech., 1965, 358–372. Stanford University Press, Palo Alto, CA*
2. **DeSoto S.** Coupled radiation, conduction, and convection in entrance region flow. *Int. J. Heat & Mass Transfer, 1968,* **11**, 39–53
3. **Pearce B. E. and Emery A.F.** Heat transfer by thermal radiation and laminar forced convection to an absorbing fluid in the entry region of a pipe. *A.S.M.E. J. Heat Transfer, 1970,* **92**(*2*), *221-230*
4. **Wassel A. T. and Edwards D. K.** Molecular radiation in a laminar or turbulent pipe flow. *A.S.M.E. J. Heat Transfer, 1976,* **98**, *101–107*
5. **Landram C. S., Grief R. and Habib I. S.** Heat transfer in turbulent pipe flow with optically thin radiation. *A.S.M.E. J. Heat Transfer, 1969,* **91**, *330–336*
6. **Clausen C. W. and Smith T. F.** Radiative and convective transfer for real gas flow through a tube with specified wall heat flux. *A.S.M.E. J. Heath Transfer, 1979,* **101**, *376–378*
7. **Smith T. F. and Clausen C. W.** Radiative and convective transfer for flow of a real gas. *Proc. 6th Int. Heat Transfer Conf., Toronto, 1978,* **3**, *391–396*
8. **Chawla T. C. and Chen S. H.** Combined radiation convection in thermally developing Poiseuille flow with scattering. *A.S.M.E. J. Heat Transfer, 1980,* ***102***, *297–302*
9. **Lii C. C. and Ozisik M. N.** Heat transfer in an absorbing, emitting and scattering slug flow between parallel plates. ASME Paper No. 73-HT-13, *A.S.M.E.-A.I.Ch.E. Heat Transfer Conf., Atlanta, GA, Aug. 1973*
10. **Viskanta R.** Interaction of heat transfer by conduction, convection, and radiation in a radiating fluid. *A.S.M.E. J. Heat Transfer, 1963,* **85**(*4*), 318–328
11. **Balakrishnan A. and Edwards D. K.** Molecular gas radiation in the thermal entrance region of a duct. *A.S.M.E. J. Heat Transfer, 1979,* **101**, *489–495*
12. **Liu S. T. and Thorsen R. S.** Combined forced convection and radiation heat transfer in the thermal entrance region of a non-isothermal parallel plate channel—optically thin gases. *A.S.M.E. Paper No. 73-HT-14, A.S.M.E.-A.I.Ch.E. Heat Transfer Conf., Atlanta, GA, Aug. 1973*
13. **Chen J. C.** Simultaneous radiative and convective heat transfer in an absorbing, emitting and scattering medium in slug flow between parallel plates. *A.I.Ch.E. J., 1964,* **2**(*2*), *253–259*
14. **Kurosaki Y.** Heat transfer by simultaneous radiation and convection in an absorbing and emitting medium in a flow between parallel plates. *Heat Transfer 1970,* 3, *4th Int. Heat Transfer Conf., Paris, 1970*
15. **Chawla T. C., Chan S. H. and Hauser G. M.** Heat transfer in thermally developing, absorbing, emitting and scattering slug and Couette flows between parallel plates with collection method. *A.S.M.E. Paper No. 79-HT-20, 1979*
16. **Greif, R. and McEligot D.** Influence of optically thin radiation on heat transfer in the thermal entrance region of a narrow duct. *A.S.M.E. J. Heat Transfer, 1971,* **93**(*4*), *473–457*
17. **Elsayed M. M. and Fathalah K. A.** Temperature distribution in direct solar heater. *A.I.Ch.E. Symp. Ser., 1980,* **76**(*198*), 62–68
18. **Fathalah K. A. and Elsayed M. M.** Natural convection due to solar radiation over a non-absorbing plate with and without heat losses. *Int. J. Heat & Fluid Flow, 1980,* **2**(*1*), 41–45
19. **Gosman A. D., Pun W. M., Runchal A. K., Spalding D. B. and Wolfshtein M.** *Heat and Mass Transfer in Recirculating Flow, 2nd edn,* 1973. *Academic Press, New York*